Wavelet imaging of transient energy localization in nonlinear systems at thermal equilibrium: The case study of NaI crystals at high temperature

Annise Rivière,[1] Stefano Lepri,[2] Daniele Colognesi,[2] and Francesco Piazza[1,*]

[1]*Université d'Orléans, Centre de Biophysique Moléculaire (CBM), CNRS UPR4301, Rue C. Sadron, 45071 Orléans, France*
[2]*Istituto dei Sistemi Complessi, Consiglio Nazionale delle Ricerche, via Madonna del Piano 10, I-50019 Sesto Fiorentino, Italy*

In this paper we introduce a method to resolve transient excitations in time-frequency space from molecular dynamics simulations. Our technique is based on continuous wavelet transform of velocity time series coupled to a threshold-dependent filtering procedure to isolate excitation events from background noise in a given spectral region. By following in time the center of mass of the reference frequency interval, the data can be easily exploited to investigate the statistics of the burst excitation dynamics, by computing, for instance, the distribution of the burst lifetimes, excitation times, amplitudes and energies. As an illustration of our method, we investigate transient excitations in the gap of NaI crystals at thermal equilibrium at different temperatures. Our results reveal complex ensembles of transient nonlinear bursts in the gap, whose lifetime and excitation rate increase with temperature. The method described in this paper is a powerful tool to investigate transient excitations in many-body systems at thermal equilibrium. Our procedure gives access to both the equilibrium and the kinetics of transient excitation processes, allowing one in principle to reconstruct the full picture of the dynamical process under examination.

I. INTRODUCTION

Hamiltonian many-body systems with nonlinear interactions admit quite generally a special class of periodic orbits, whose amplitude-dependent frequency does not resonate by construction with any of the linear (normal) modes (NM) and whose oscillation pattern is typically exponentially localized in space. These modes, termed discrete breathers (DB) [1–3] or intrinsic localized modes (ILM) [4], have been shown theoretically to exist at zero temperature in a wide range of systems, including model lattices of beads and springs, such as the celebrated Fermi-Pasta-Ulam (FPU) chain [5], real 2D and 3D crystals [6], both in the gap [7] and above the phonon spectrum [8], including cuprate high-T_c superconductors [9], boron nitride [10], graphene [11–13] and diamond [14], disordered media [15–17], and biomolecules [18] including proteins [19,20]. Nonlinear modes of this kind are surmised to play a subtle role in many condensed-matter systems. For example, DBs have been found to be connected to negative-temperature states (i.e., states for which the derivative of entropy versus energy is negative) in the discrete nonlinear Schrödinger equation [21], which is relevant to the physics of Bose-Einstein condensates in optical lattices and arrays of optical waveguides. ILMs have also been surmised to accelerate the kinetics of defect annealing in solids [22] and more generally to speed up heterogeneous catalysis processes [23,24].

If zero-temperature nonlinear excitations are well-established and fairly understood physical objects, when it comes to systems at thermal equilibrium the scenario

proves far more complex and thorny [25]. Numerical techniques based on spectral analyses coupled to surface cooling techniques have been proposed as means to detect spontaneous DB excitation in model nonlinear lattices [26]. More recently, other studies have also addressed this problem via equilibrium MD simulations, both in model nonlinear chains [27] and in crystals with realistic potentials ranging from graphane [28,29] to crystals with the NaCl structure [30].

Experimental evidence for nonlinear localized excitations is no less a spinous matter. Nonlinear localized modes have been found experimentally at finite temperature in Josephson ladders [31] and arrays [32]. However, the oldest experimental evidence explained in terms of excitation of ILMs at finite temperature in a crystal are the elusive tracks arising from nuclear scattering events in muscovite mica [33]. Such dark lines, known since a long time [34], have led to the suggestion that ILMs might act as energy carriers in crystals along specific directions with minimal lateral spreading and over long distances [35]. Recently, experimental evidence has been collected in support of this inference, as infinite charge mobility has been measured at room temperature in muscovite mica crystals irradiated with high-energy alpha particles [36].

Indirect evidence for the nonequilibrium excitation of ILMs at finite temperature has been also gathered through inelastic x-ray and neutron scattering measurements on α-uranium single crystals [37,38]. In particular, the authors of these studies speculate that the excitation of mobile modes, whose properties are consistent with those of ILMs, could explain the measured anisotropy of thermal expansion and the deviation of heat capacity from the theoretical prediction at high temperatures [39]. More recently, the same authors have published experimental evidence of the excitation of intrinsic

*Francesco.Piazza@cnrs-orleans.fr

localized modes in the high-temperature vibrational spectrum of NaI crystals [40], where ILMs have been predicted to exist at $T = 0$ and characterized by many authors [7,30,41–43]. In 2011, the same authors published time-of-flight inelastic neutron scattering measurements performed on NaI single crystals [44]. Their results seemed to point at the spontaneous thermal excitation of ILMs, moving back and forth between the [111] and [011] orientations at intermediate temperatures and eventually locking in along the [011] orientation above $T = 636$ K. Further inelastic neutron scattering measurements on NaI crystals published in 2014 found no evidence for thermally activated localized modes [45]. Even though these measurements confirmed a very small peak within the gap, its intensity is so small—the authors argue—that it is nearly impossible to discern whether it is part of the inelastic background or whether it is indeed a true signature of a coherent scattering event. However, in a subsequent paper [46], Manley and coworkers made it clear that the interpretation of the coherent scattering from NaI requires a correction of the incoherent background from the incoherent cross section of Na, which was not included in Ref. [45]. As the partial phonon DOS of Na displays a stretch of reduced intensity at high temperatures in the spectral region corresponding to the $T = 0$ gap, when this correction is made (as in Ref. [46]), the ILM feature becomes a little more pronounced. Combining neutron scattering, laser flash calorimetry and accurate x-ray diffraction data, the authors then argued that ILM localization in NaI occurs in randomly stacked planes perpendicular to the (110) direction(s) with a complex temperature dependence [46]. As a result, they suggested that spontaneous localization of ILMs should be regarded as some sort of collective phenomenon rather than the random excitation of pointlike modes.

To this complex scenario, one should add that the expected relative fraction of light ions harboring a thermally excited ILM in NaI is relatively low. As an example, the prediction made in Ref. [41] for ILMs polarized along the [111] orientation at $T = 636$ K is about 8.3×10^{-4}, which would make their direct observation a very hard matter.

Taken together, the facts exposed above reveal a lively albeit rather intricate debate concerning the very existence of thermal ILMs in crystals and the means to possibly spotlight their presence and characterize them. In order to address these questions, in this paper we develop a robust numerical technique based on continuous wavelet analysis, designed as a tool to pinpoint and characterize transient vibrational excitations, in general, in many-body system, and illustrate it in the case of NaI crystals. The paper is organized as follows. In Sec. II, we describe the MD simulation protocol and present our wavelet-based technique designed to pinpoint and characterize transient energy bursts in the time-frequency plane. In Sec. III, we apply our technique to characterize transient excitation of energy in the gap of NaI crystals. In Sec. IV, based on the assumption that the population of transient energy bursts detected in the gap may contain spontaneous excitation events of ILMs, we address the problem of how to sieve them out of the burst population. In Sec. V, we summarize our main findings and discuss possible improvements and extensions of our method to detect and characterize spontaneous excitation of ILMs at thermal equilibrium.

II. SIMULATIONS AND WAVELET ANALYSIS

In order to illustrate our approach, we have used the molecular simulation (MD) engine LAMMPS [47] to simulate the equilibrium dynamics of a NaI crystal as a function of temperature. The simulation box comprises N_c^3 cubic unit cells with periodic boundary conditions (PBC) along the three Cartesian directions, each cell containing $4 \, \mathrm{Na}^+$ and $4 \, \mathrm{I}^-$ ions. For all simulations reported here, we have taken $N_c = 10$, so that the total number of ions is 8000.[1] The choice of interatomic potentials is crucial. In order to determine the best available choice, we have scrutinized a large body of specialized literature [48–57], which led us to reconstruct a total potential energy of the form

$$U(\{\mathbf{r}, \mathbf{R}\}) = \sum_{i>j} V_{++}(|\mathbf{R}_i - \mathbf{R}_j|) + \sum_{i>j} V_{--}(|\mathbf{r}_i - \mathbf{r}_j|) + \sum_{i,j} V_{+-}(|\mathbf{R}_i - \mathbf{r}_j|), \quad (1)$$

where $\mathbf{R}_i$ and $\mathbf{r}_i$ denote the position vectors of Na^+ and I^- ions, respectively. Each pairwise contribution comprises three terms,

$$V_{\pm\pm}(r) = \frac{Q_\pm Q_\pm}{4\pi\epsilon_0 r} + W_{\pm\pm}^{LR}(r) + P_{\pm\pm}^{SR}(r). \quad (2)$$

The Coulomb energy has been computed via the Ewald method [58]. Instead of specifying a cutoff wave vector for the Ewald sums, we have set the relative error in the calculation of electrostatic forces to be less than 10^{-5} at any given time. We have verified that our results did not change by requiring a more accurate estimation. The potential energy W^{LR} accounts for a long-range potential of the (6,8) kind, namely,

$$W_{\pm\pm}^{LR}(r) = -\frac{C_\pm}{r^6} - \frac{D_\pm}{r^8} \quad (3)$$

corresponding to induced dipole-induced dipole interactions $(C_\pm)$ and induced dipole-induced quadrupole interactions $(D_\pm)$ computed via the Kirkwood-Muller methods, i.e., using experimental measurements of the ionic polarizability and molar susceptibility [59,60]. The short-range term is well described by a Buckingham-type potential [61] of the form

$$P_{\pm\pm}^{SR}(r) = A_{\pm\pm} \exp(-r/\rho_{\pm\pm}) \quad (4)$$

restricted to the nearest-neighbor shell (5 Å cutoff). The values of the parameters in Eqs. (3) and (4) are listed in Table I.

Since the lattice constant of NaI crystals is known experimentally and has been used, alongside other experimentally determined constants, to parametrize the potential energy (1) [48–57], we have used these measurements to set the dimension of the unit cell at different temperatures and performed fixed-volume simulations. A typical simulation consisted of a first thermalization NVT stage of duration Δt_{th}, where

----

[1]We observe that PBCs with $N_c = 10$ appears a safe choice to inspect energy localization on length scales of the order of half/one unit cell.

TABLE I. Parameters of the pair-wise short-range and long-range potential energies used in this study to simulate the dynamics a NaI crystal. For more information, see Refs. [48–57].

Pair kind	Short range		Long range	
	$A_{\pm,\pm}$ (eV)	$\rho_{\pm\pm}$ (Å)	$C_{\pm,\pm}$ (eV Å^6)	$D_{\pm,\pm}$ (eV Å^8)
++	8500.74	0.29333	4.93337	3.55827
−−	384.924	0.50867	810.714	805.769
+−	736.498	0.40100	54.9164	47.0954

the system was brought to thermal equilibrium through a Nosé-Hoover thermostat [62,63] starting from zero initial atomic displacements and random velocities drawn from a Maxwell distribution. We have verified that $\Delta t_{th} = 5$ ps was sufficient to correctly thermalize our system for temperatures larger than 400 K. Once the system is thermalized, we run constant energy trajectories (NVE) of duration Δt_p for data production. It is interesting to remark that distortions driven by the localization of nonlinear vibrational modes are expected to conserve volume, as it was found for the internal distortions associated with ILM localization in the faultlike planar structures reported in Ref. [46].[2] The results presented in the following refer to $\Delta t_p = 100$ ps, which afforded a reasonable compromise between computational costs and solid statistics. The time step used in the MD simulations was 0.001 ps.

Figure 1 illustrates the comparison of the low-temperature phonon density of states computed by Fourier transforming the velocity-velocity autocorrelation functions computed from our LAMMPS NVT trajectories with the results from lattice dynamics calculations performed with the GULP package [64]. The excellent agreement validates our MD simulation protocol and in particular the values of the phonon frequencies that define the gap at zero temperature, i.e., $\omega_1 = 16.104$ ps^{-1} (upper edge of the acoustic band) and $\omega_2 = 20.343$ ps^{-1} (lower edge of the optical band).

A. Wavelet imaging of transient energy bursts in the gap

Wavelet analysis is the ideal tool to analyze nonstationary signals in the time-frequency domain in order to characterize transient frequency components appearing at specific times and perduring for finite lapses of time. As a matter of fact, Forinash and co-workers have shown 20 years ago that this

---

[2]The use of an NVT dynamics for production runs does not appear to make sense in this study. In fact, thermostats are, in principle, nothing but *smart sampling* techniques, designed to produce time series sampled from the canonical measure. However, there is absolutely no guarantee that the actual trajectories (i.e., the actual *dynamics*) make any physical sense. In particular, all vibrational coherences are either (artificially) damped or completely destroyed, depending on the value of the relaxation time scale chosen for the specific thermostat. In practice, it is preferable to switch off the thermostat once the system has reached thermal equilibrium, so that no artificial noise is left to fiddle with the vibrational coherences that might emerge in specific frequency regions.
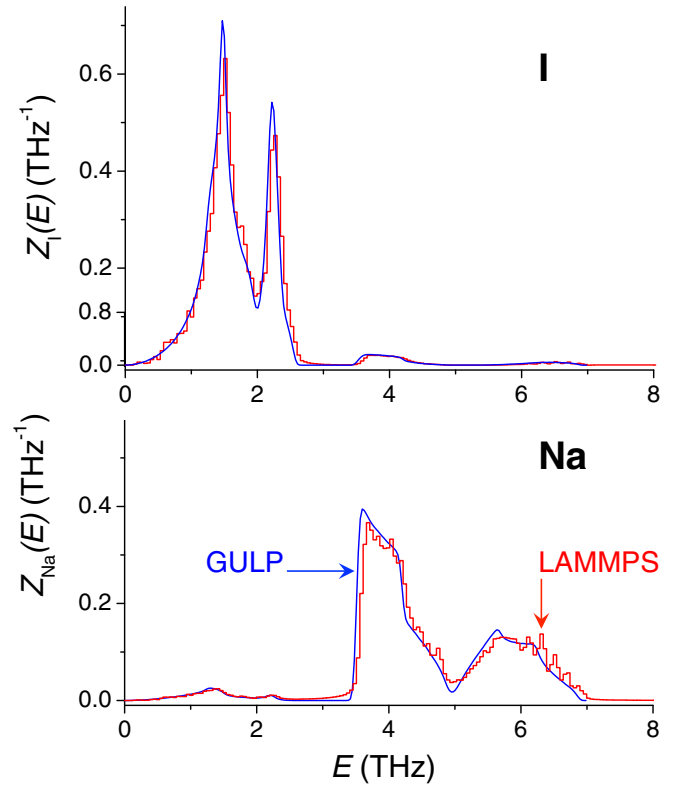
FIG. 1. Phonon DOS of NaI computed from NVE MD simulations ($T = 38$ K, LAMMPS, red staircases) and from lattice dynamics calculations ($T = 77$ K, GULP, blue lines). The energy $E = h\nu$ is measured in units of the frequency ν.

kind of tools can provide precious information on the dynamics of discrete breathers at zero temperature in nonlinear chains [65]. Thus, it appears natural to extend this line of reasoning to explore transient nonlinear localization in real crystals at thermal equilibrium. In this work, we have computed the Gabor transform [66] of the time series of atomic velocities, namely,

$$G_{i\alpha}(\omega, t) = \int_{-\infty}^{+\infty} e^{-(t-\tau-\Delta t_p/2)^2/a} e^{-i\omega\tau} v_{i\alpha}(\tau)\, d\tau, \quad (5)$$

where $v_{i\alpha}$ is the velocity of the ith ion along the Cartesian direction α. We have set the resolution parameter $a = 20$ ps^2, optimized so as to maximize the resolution in both the time and frequency domains.

As an illustration of our analysis, Fig. 2 shows typical density maps of $|G_{i\alpha}(\omega, t)|^2$ computed from the velocity time series of two random Na ions at $T = 600$ and 900 K. It can be appreciated that, as the temperature increases, transient energy bursts pop up increasingly deep in the gap and persist with lifetimes of the order of up to 10 ps, during which their frequency appears to drift to a various degree. In order to separate energy bursts from the background and perform a full temperature-dependent statistical analysis of the excitation dynamics, it appears natural to impose a threshold P_G on the Gabor power so as to eliminate transient background noise. To this end, we define the filtered normalized two-dimensional
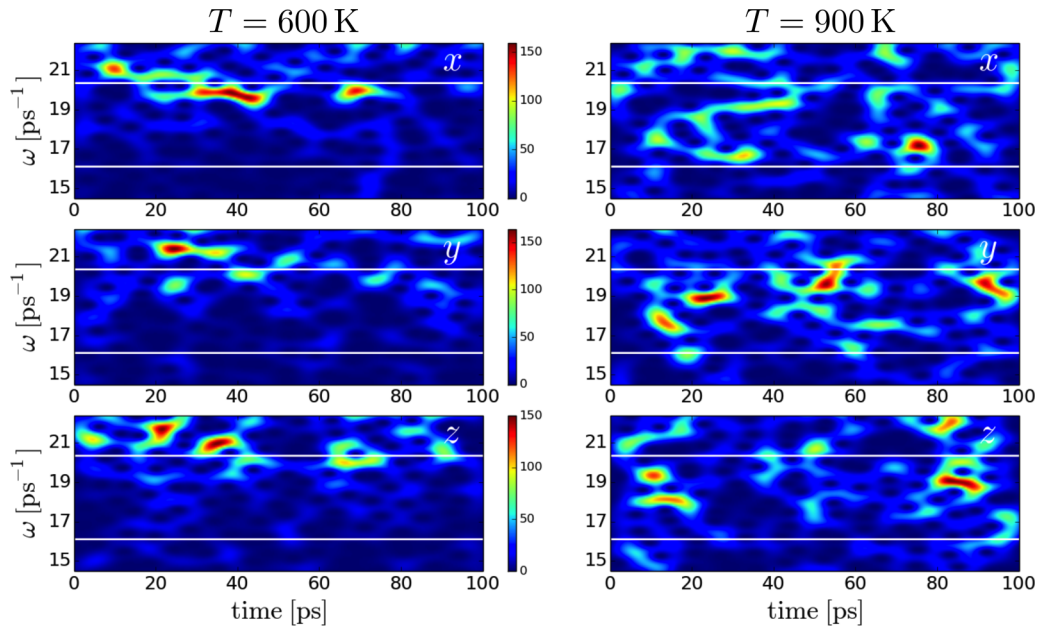
FIG. 2. Time-frequency density maps of the function $|G_{i\alpha}(\omega,t)|^2$ in the gap region for two different Na ions at $T = 600$ and 900 K along the three Cartesian directions (x, y, z from top to bottom). Spectral power is color-coded from blue (low energy) to red (high energy). The two horizontal white lines mark the edges ω_1, ω_2 of the gap region.

excitation density $\rho_{i\alpha}(\omega,t)$ as

$$\rho_{i\alpha}(\omega,t) = \frac{|\widetilde{G}_{i\alpha}(\omega,t)|^2}{\int_{\omega_2}^{\omega_1} |\widetilde{G}_{i\alpha}(\omega',t)|^2 \, d\omega'}, \qquad (6)$$

where

$$\widetilde{G}_{i\alpha}(\omega,t) = \begin{cases} G_{i\alpha}(\omega,t) & \text{for} \quad |G_{i\alpha}(\omega,t)|^2 \geqslant P_G \\ 0 & \text{otherwise} \end{cases}. \qquad (7)$$

This definition allows us to compute the time-dependent moments of $\rho_{i\alpha}(\omega,t)$, which provide important information on the dynamics of transient energy excitation in the gap. In the present work, we concentrate on the first moment, namely,

$$\langle \omega_{i\alpha}(t) \rangle = \int_{\omega_1}^{\omega_2} \omega \rho_{i\alpha}(\omega,t) \, d\omega. \qquad (8)$$

As it can be seen from the top panel in Fig. 3, the choice of the threshold P_G sets the resolution limit of individual burst events. After careful examination of many such events, we have fixed $P_G = 128$ Å^2, which ensures that consecutive bursts should be optimally resolved. Although the results reported in the following refer to this (rather conservative) choice, we have repeated our analyses with the two lower values of P_G shown Fig. 3. While the actual figures may change slightly, we have verified that the relevant statistical and physical properties of the burst excitation dynamics are unchanged.

After the filtering and integration procedure for a given ion i, the time series $\langle \omega_{i\alpha}(t) \rangle$ are piecewise composed of stretches of consecutive zeros (absence of a burst) and consecutive nonzero values, each representing a burst and extending over its corresponding lifetime. Such values describe the drift of the center-of-mass frequency of the burst since the moment of its excitation until it collapses. From the support of these time series, it is then straightforward to obtain other restricted time series *per burst*, most importantly the sequences of kinetic

energies and vibration amplitudes for each burst during its lifetime.

III. RESULTS I: TRANSIENT ENERGY BURSTS IN THE GAP WITH INCREASING LIFETIMES

Nonlinear localized vibrations in the gap of diatomic lattices detach from the bottom of the optical band [67], which means that their energy is almost entirely confined to light ions. For a given Na ion, two key kinetics parameters describe the burst excitation dynamics, notably the lifetimes t_n and the excitation times τ_{n+1}, $n = 0, 1, 2, \ldots$ These two measures are illustrated in the middle panel in Fig. 3 for a random typical excitation sequence. The excitation times are defined as the intervals between consecutive excitation events. Together with the lifetimes, they provide a rich wealth of information on the kinetics of burst excitation at a given temperature. However, irrespective of the kinetics, the temperature dependence of the site-occupancy probability (SOP) $\mathcal{P}(T)$ describes the equilibrium properties of this process. This can be simply computed as the fraction of Na ions harboring at least one burst in the gap along one of the Cartesian directions.[3] The data, reported in Fig. 4 (top left), can be fitted by a simple equilibrium model of the kind

$$\mathcal{P}(T) = \frac{1}{1 + e^{\beta \Delta f}}, \qquad (9)$$

where $\beta = 1/k_B T$ and $\Delta f = \Delta \epsilon - T \Delta s$ is the free energy of burst excitation per ion. The excellent fit of the MD simulation data gives $\Delta \epsilon = 0.54 \pm 0.01$ eV and $\Delta s = 9 \pm 0.2 \, k_B$. The data reported in Fig. 4 are obtained by averaging the site-

---

[3]In this work, we implicitly refer to the gap spectral region when we mention the excitation of a burst.
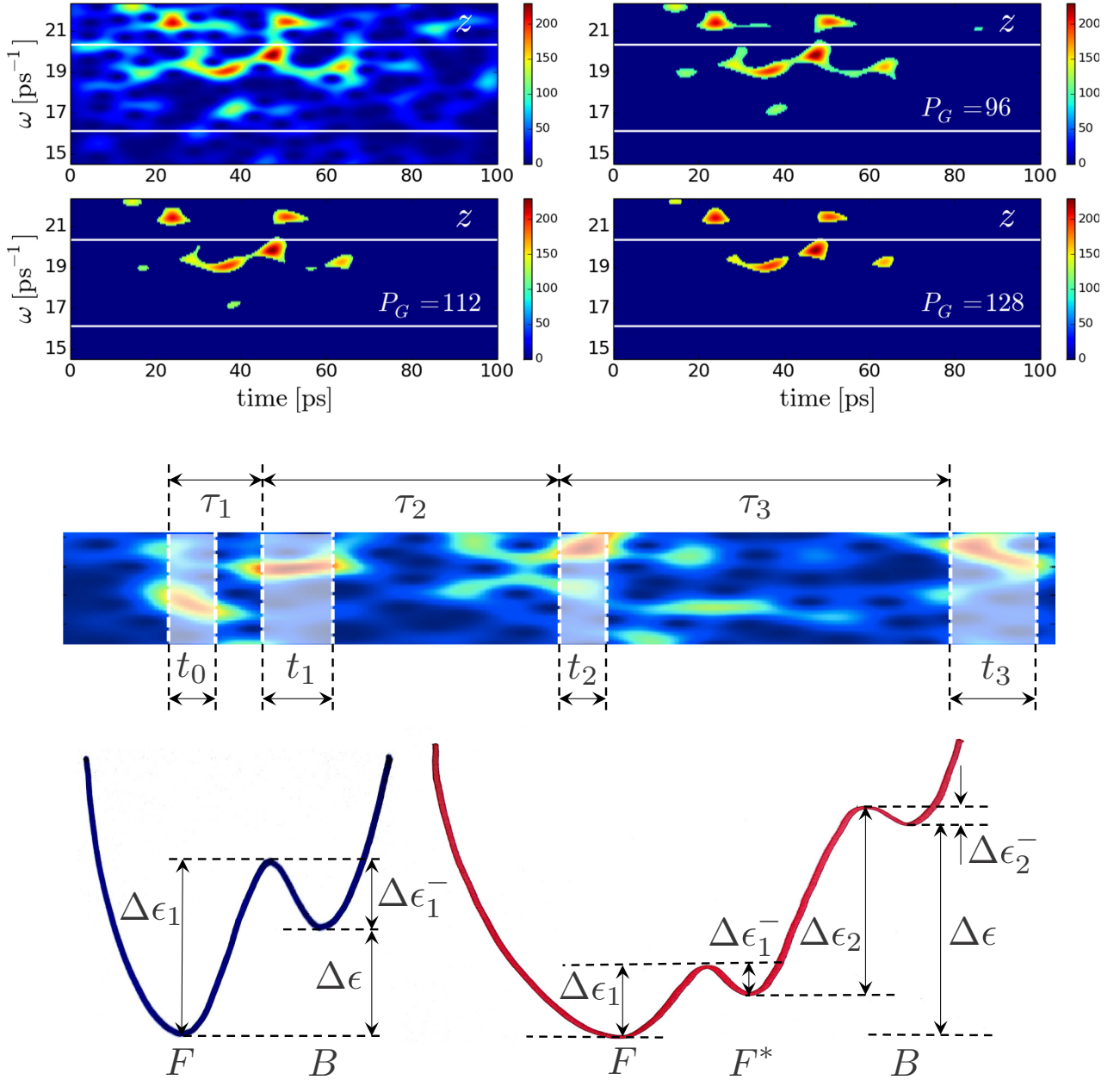
FIG. 3. (Top) Illustration of the filtering procedure to isolate energy bursts with three different thresholds (units of Å^2). (Middle) Scheme of the algorithm to identify lifetimes t_n and excitation times τ_n during the production run Δt_p for a given ion from the time series of $\langle \omega_{i\alpha}(t) \rangle$ defined in Eq. (8). (Bottom left) Kinetic model based on a two-well landscape fails to reproduce the kinetics and equilibrium properties of burst excitation. (Bottom right) At least one intermediate state is required to rationalize the kinetics and equilibrium of the thermally activated process of burst generation. This profile reproduces to scale a possible three-well landscape that is in agreement with our simulation data. The energy scale that controls the burst lifetimes in this picture is $\delta \epsilon := (\Delta \epsilon_1 - \Delta \epsilon_1^-) - \Delta \epsilon_2^-$ (see extended discussion in the text).

occupancy probabilities referring to bursts along individual Cartesian directions. However, we observe that the three individual SOPs are indistinguishable from one another (data not shown), which appears natural in view of the symmetry of the crystal.

It is interesting to note that the simple law (9) was found to describe the excitation of ILMs along [111] in Ref. [41], with $\Delta \epsilon = 0.608$ eV and $\Delta s = 4 \, k_B$, corresponding to the four symmetry-equivalent L points at the boundary of the Brillouin zone (BZ) from which an ILM can in principle detach with a [111] polarization. In our case, we only expect a small fraction

of the bursts to possibly be transient excitations of ILMs. It is nonetheless interesting to observe that the excitation energy that we find is close to a very good guess for an ILM in 3D NaI. Furthermore, the value $\Delta s = 9 \, k_B$ is close to the overall symmetry degeneracy of the L, K, and X points in the BZ taken together, i.e., 10, corresponding to the extra degeneracy associated with the theoretical conversion points to ILMs along [110] (K) and along [100] (X). Of course, if this interpretation has some truth to it, it seems that the three kinds of ILMs might be excited at the same time and possibly move as units back-and-forth among them, as already speculated
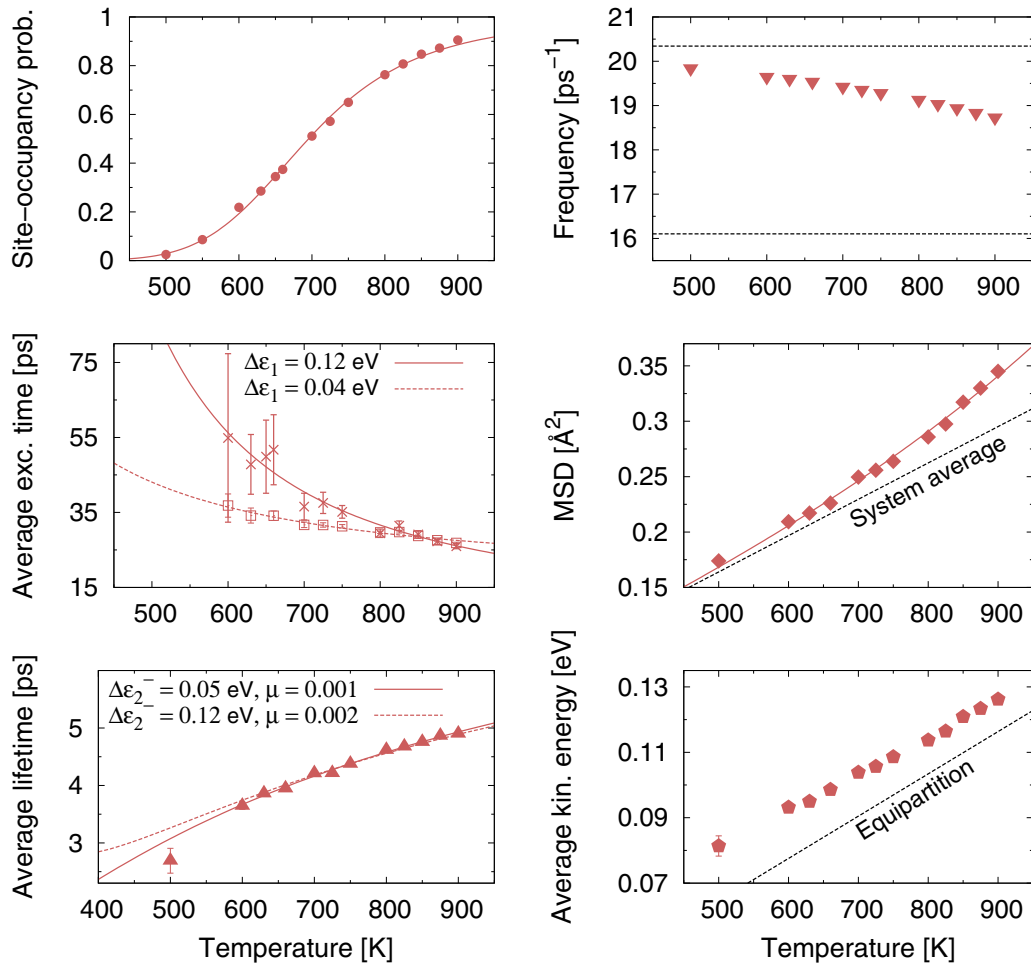
FIG. 4. Analysis of the burst excitation equilibrium, kinetics, and dynamics. (Top left) Equilibrium burst site-occupancy probability at Na ions vs temperature from the simulations (filled circles) and fit with the chemical equilibrium model (9). Best-fit parameters are $\Delta\epsilon = 0.54 \pm 0.01$ eV, $\Delta s = 9 \pm 0.2\, k_B$. (Middle left) Average excitation times (see again Fig. 3) identified from the support of the filtered integrated time series (8). Open squares represent the average values computed over all the pairs of consecutive excitation events, further averaged over x, y, and z. The crosses represent the values computed by fitting the exponential tails of the distributions and rescaled so as to match the high-temperature averages. This set of data is likely to better approximate the true values at low temperatures. The two lines are plot best-fit Arrhenius laws of the kind (12). Best fit parameters are $\Delta\epsilon_1 = 0.12 \pm 0.1$ eV, $k_1^\infty = 0.18 \pm 0.03$ ps^{-1} (solid line) and $\Delta\epsilon_1 = 0.04 \pm 0.02$ eV, $k_1^\infty = 0.06 \pm 0.005$ ps^{-1} (dashed line). The *true* value of $\Delta\epsilon_1$ (i.e., the average computed over a simulation long enough to sample very long excitation times) is expected to be in the interval [0.04, 0.12] eV. (Bottom left) Average lifetimes (see again Fig. 3) identified from the support of the filtered integrated time series (8) (symbols) and fits with the three-states model expression (18). The solid line is a three-parameter fit, where the floating parameters are t_∞, $\delta\epsilon := (\Delta\epsilon_1 - \Delta\epsilon_1^-) - \Delta\epsilon_2^-$, $\mu = k_{-1}^\infty / k_1^\infty$ and $\Delta\epsilon_2^-$ is kept fixed at 0.04 eV. The dashed line is a two-parameter fit, where $\Delta\epsilon_2^-$ is kept fixed at 0.1 eV, while this time the energy scale that physically controls the increasing trend, $\delta\epsilon$, is kept fixed at the previous best-fit value, i.e., $\delta\epsilon = 0.07$ eV (see text for the full discussion). (Top right) Average burst frequencies vs temperature. (Middle right) Average burst amplitude vs temperature (filled diamonds) and average amplitude of the fluctuations of all Na ions in the system (dashed straight line). The solid line is a fit with a function of the kind $\langle A^2(T) \rangle = \alpha T + \beta T^4$, intended as a guide to the eye. (Bottom right) Average burst kinetic energy vs temperature (filled pentagons), i.e., ensemble average of the individual burst energies. The dashed line marks the equilibrium value $\langle \epsilon_{\text{kin}} \rangle = 3k_B T/2$. At each temperature, the reported average frequencies, amplitudes, and kinetic energies represent the ensemble averages of the *individual* average values *per burst*. The latter are computed by averaging over the individual drift of each single burst, as identified from the support of the corresponding filtered time series (8). We remind the reader that each burst is associated with a single Na ion and Cartesian direction.

by Manley and co-workers for the interplay of [110] and [111] ILMs below 636 K [44]. We observe, however, that this kind of complex dynamics would appear exceedingly difficult to disentangle, even in the framework of a computational study like this, as confirmed by the indistinguishability of the SOPs describing burst excitation along individual Cartesian directions.

From the point of view of chemical kinetics, the expression (9) describes the equilibrium between two species/states with an arbitrary number of intermediates. It is tempting to follow this lead to get some insight into the burst excitation process. In the simplest possible scenario, we would be dealing with two states, F and B, describing random energy fluctuations (F) and energy fluctuations within a burst (B). In the

framework of this simple mean-field description, the time evolution of the site-occupancy probability would be given to a first approximation by

$$\frac{\partial \mathcal{P}(T,t)}{\partial t} = k_1[1 - \mathcal{P}(T,t)] - k_{-1}\mathcal{P}(T,t), \quad (10)$$

where k_1 and k_{-1} stand for the burst birth and death rates, respectively. In this picture, one immediately sees that the equilibrium site-occupancy probability is simply given by

$$\mathcal{P}(T) = \frac{1}{1 + k_{-1}/k_1}, \quad (11)$$

where k_{-1}/k_1 is the effective *dissociation* constant of the $F - B$ equilibrium. In a simple picture described by an energy landscape with two minima (Fig. 3, bottom left), the excitation energy $\Delta\epsilon$ would just be the difference between the two excitation barriers $\Delta\epsilon_1$ ($F \rightarrow B$) and $\Delta\epsilon_1^-$ ($B \rightarrow F$), defined by Arrhenius-like laws of the kind

$$k_1 = k_1^\infty e^{-\beta\Delta\epsilon_1}, \quad (12)$$

$$k_{-1} = k_{-1}^\infty e^{-\beta\Delta\epsilon_1^-}. \quad (13)$$

In this model, $\Delta\epsilon = \Delta\epsilon_1 - \Delta\epsilon_1^- < \Delta\epsilon_1$ and $\Delta s = \ln(k_{-1}^\infty/k_1^\infty)$. However, a quantitative analysis of our data reveals that the best estimate of the excitation energy is $\Delta\epsilon_1 = 0.12 \pm 0.1$ eV, which is *lower* than $\Delta\epsilon$ (middle left panel in Fig. 4). It should be stressed that the numerical determination of average excitation times is a delicate matter, for long excitation times are clearly under-represented in the population of recorded events (i.e., pairs of consecutive excitations). In fact, the population observed in a simulation is obviously cut off at $\tau = \Delta t_p$. This means that the observed averages $\langle\tau(T)\rangle$ are underestimated at the lower temperatures, where excitation times are longer. In order to gauge this effect, it is expedient to fit the exponential tail of the numerical distributions before the cutoff. The temperature trend of such decay times, lower in value than the corresponding averages, should nonetheless be a good representation of the *true* trend (i.e that of averages computed from infinitely long simulations). The middle panel in Fig. 4 shows that this seems, indeed, to be the case, placing the value of the excitation energy $\Delta\epsilon_1$ somewhere in the interval [0.04, 0.12] eV.

The fact that $\Delta\epsilon_1 < \Delta\epsilon$ rules out a simple two-minima picture. To complicate the picture further, it can be seen from Fig. 4 (bottom left panel) that the average burst lifetimes are found to *increase* with temperature, in agreement with previous results of MD simulations in crystals with the NaCl structure at thermal equilibrium [68]. As a matter of fact, we found that the distribution of burst lifetimes extends to longer and longer times (up to lifetimes of the order of 20–30 ps) as the temperature increases (see Fig. 5).These somewhat counterintuitive results are also incompatible with a two-well free energy landscape, which would predict $\langle t(T)\rangle \propto 1/k_{-1}$ and therefore lifetimes decreasing with temperature, as escaping from the B state becomes more and more favored at higher temperatures as prescribed by Eq. (13).

Of course, one might invoke general nonlinear effects to explain the observed increase in self-stabilization of bursts at increasing temperatures. However, it is not clear how this
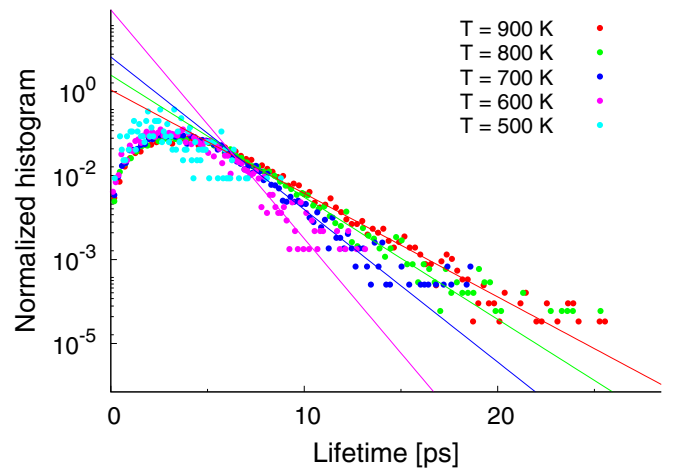
FIG. 5. Distributions of burst lifetimes at five representative temperatures (symbols). The solid lines are plots of exponential fits to the distribution tails.

can be quantified in simple terms. In this paper, we explore another route that provides an effective description of the burst excitation dynamics and has the advantage of sketching a general interpretative paradigm to combine equilibrium and kinetics observables.

ILM/DB excitation is expected to be a thermally activated phenomenon, in view of the general existence of excitation thresholds in nonlinear lattices [69,70]. This has been confirmed explicitly for spontaneous excitation of DBs in the framework of surface-cooling numerical experiments in 2D FPU lattices [71]. If one sticks to the physics of a thermally activated process occurring along some reaction coordinate, in order to rationalize the observed burst excitation process, it is necessary to introduce at least an intermediate state, F^*, according to the kinetic model

$$F \underset{k_{-1}}{\overset{k_1}{\rightleftharpoons}} F^* \underset{k_{-2}}{\overset{k_2}{\rightleftharpoons}} B. \quad (14)$$
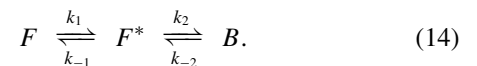
The state F^* could be interpreted as a precursor fluctuation that can be either stabilized—this is where nonlinear effects come into play in this picture—to yield a persistent burst, or it can decay back into the background. As we shall see in the following, the obvious coming into play of nonlinear effects as temperature increases is confirmed by the observed trend of the burst average amplitudes. The scheme (14) corresponds to a three-minima landscape as illustrated in Fig. 3 (bottom right panel). The relative equilibrium population of the B state, i.e., the burst site-occupancy probability $\mathcal{P}$ in our analogy, can be simply computed by imposing the detailed-balance conditions $k_1 F_e = k_{-1} F_e^*$ and $k_2 F_e^* = k_{-2} B_e$. This yields immediately

$$\mathcal{P} \equiv \frac{B_e}{F_e + F_e^* + B_e} = \frac{1}{1 + \dfrac{k_{-2}(k_1 + k_{-1})}{k_1 k_2}}. \quad (15)$$

In this model, the burst lifetime is set by the rate k_{-2}. With reference to the landscape depicted in the bottom right panel in Fig. 3, let us take $\langle t(T)\rangle \propto 1/k_{-2}$ and let us assume that k_2 and k_{-2} are described by Arrhenius expressions such as (12) and (13) [i.e., $k_2 = k_2^\infty \exp(-\beta\Delta\epsilon_2)$,

$k_{-2} = k_{-2}^\infty \exp(-\beta \Delta \epsilon_2^-)$]. Then, comparing Eqs. (15) and (9), we are led immediately to the following expression:

$$\langle t(T) \rangle = t_\infty \left(\frac{1 + \mu\, e^{\beta \Delta \Delta \epsilon_1}}{1 + \mu} \right) e^{-\beta(\Delta \Delta \epsilon_1 - \Delta \epsilon_2^-)}, \qquad (16)$$

where $\Delta\Delta\epsilon_1 := \Delta\epsilon_1 - \Delta\epsilon_1^-$, $\mu = k_{-1}^\infty / k_1^\infty$, and t_∞ is the asymptotic, infinite-temperature lifetime ($\propto 1/k_{-2}^\infty$) determined uniquely by the kinetic (entropic) constants (see again the three-well landscape pictured in Fig. 3).

The function (16) is a monotonically decreasing function of temperature or features a minimum at low temperatures and an increasing trend for higher temperatures depending on the relative value of the relevant kinetic and energy scales. More precisely, an increasing portion at high temperature will be observed provided $(\Delta\Delta_1 - \Delta\epsilon_2^-)/\Delta\epsilon_2^- > \mu$, that is,

$$\frac{\Delta\epsilon_1 - \Delta\epsilon_1^-}{\Delta\epsilon_2^-} > 1 + \frac{k_{-1}^\infty}{k_1^\infty}. \qquad (17)$$

It should be observed that no bursts in the gap are observed in our simulations below 500 K (see again the top left panel in Fig. 4). This is consistent with a barrier $\Delta\epsilon_1$ in the 0.1 eV ballpark (at 500 K the average kinetic energy per particle would yield a rate $k_1 \approx 0.1 k_1^\infty$). Thus the three-wells free energy landscape sketched in Fig. 3 should be considered as describing the stabilization of fluctuations for temperatures $\gtrsim 500$ K. The two barriers should be imagined as being vanishingly small at lower temperatures, where, at most, fluctuations might be described by a simple two-state $F - F^*$ equilibrium. This is the regime where bursts become short-lived and make only rare appearances in the gap, most likely, close to the bottom of the optical band (see again the left panel in Fig. 2).

We see from the condition (17) that, physically, increasing burst lifetimes at high temperatures arise as a combination of (i) slow decay kinetics of the intermediate state F^*, (ii) large values of the energy describing the $F - F^*$ equilibrium, $\Delta\epsilon_1 - \Delta\epsilon_1^-$, and small values of the energy barrier for the decay of the B state, $\Delta\epsilon_2^-$. In particular, if the velocity constant of the $F^* \to F$ de-excitation is much slower than the velocity of the first excitation, $F \to F^*$ (i.e., a large positive entropy difference in favor of the F^* state), then the term proportional to μ can be neglected and the burst lifetime will be an increasing function of temperature over the whole physically meaningful temperature range, as controlled solely by the positive energy difference $(\Delta\epsilon_1 - \Delta\epsilon_1^-) - \Delta\epsilon_2^-$.

From a practical standpoint, due to the short temperature stretch available to fit the numerical data and the functional form (16), it is not possible to fit meaningfully all the unknown parameters in Eq. (16). However, the energy scale controlling the increasing trend is $\delta\epsilon := (\Delta\epsilon_1 - \Delta\epsilon_1^-) - \Delta\epsilon_2^-$. Hence the agreement of this simple kinetic mean-field theory with the simulations can be assessed by fixing the unknown barrier $\Delta\epsilon_2^-$ and fitting a functional form of the kind

$$\langle t(T) \rangle = t_\infty \left(\frac{e^{-\beta\delta\epsilon} + \mu\, e^{\beta\Delta\epsilon_2^-}}{1 + \mu} \right) \qquad (18)$$

with t_∞, μ, and $\delta\epsilon$ free to float. For example, with $\Delta\epsilon_2^- = 0.04$ eV, we get $\mu = 0.06 \pm 0.03$, $\delta\epsilon = 0.07 \pm 0.03$ eV, and $t_\infty = 10 \pm 2$ ps. To obtain a more meaningful assessment,

we repeated the fit by fixing the barrier to a different value, $\Delta\epsilon_2^- = 0.1$ eV, and kept $\delta\epsilon = 0.07$ eV from the first fit. It is clear from Fig. 4 that the theory still describes the simulation data in the observed temperature range. In this case, we get consistent values of the two floating parameters left, namely $\mu = 0.013 \pm 0.03$ and $t_\infty = 11.5 \pm 0.2$ ps.

The top right panel in Fig. 4 shows the average frequency of bursts as a function of temperature. Of course, the lower edge of the phonon optical band is expected to soften, hence it is difficult to disentangle nonlinear phonon frequencies from possible ILM events from these average data as the gap gets progressively colonized by soft nonlinear phonons. In the following, we will discuss this point further and point to a possible strategy to get more insight as to ILM signatures.

At variance with the average frequencies, an analysis of the average vibrational amplitudes of bursts in the gap reveal a telltale sign of nonlinear effects. In the middle right panel in Fig. 4, we compare the mean square displacement (MSD) computed over all Na ions in the crystal with the average MSD of Na ions hosting a burst (i.e., the mean over the burst population of the average MSD of each burst, the latter being computed over its corresponding lifetime). It is clear that, starting from temperatures of the order 500 K, bursts clearly vibrate with increasing amplitudes, detaching from the harmonic $\propto T$ law. This seems to indicate that bursts of energy in the gap are intrinsically nonlinear excitations.

Another rather puzzling piece of information comes from the analysis of the average burst kinetic energies (lower right panel in Fig. 4). These turn out to follow a linear trend, as the equipartition theorem would prescribe for each and every Na ion in the system, however, the average energies seem to be proportional to an *effective* temperature that is about 100 K higher than the true one (see the dashed line in the lower right panel of Fig. 4). In other words, during the lifetime of a burst, the corresponding Na ion has on average systematically a higher energy than the average Na ion in the system. This is in agreement with the behavior of the MSD. If one surmises that the fraction of bursts that display characteristics typical of ILMs is non-negligible, a possible explanation of these effects might reside in the known tell-tale ability of ILMs to harvest energy from the background by absorbing lower-energy radiation [2,71]. Pushing this line of reasoning further, the origin of the observed higher-than-average energies of bursts in the gap might reveal a sheer nonlinear self-stabilization process akin to the well-known ILM behavior during surface cooling [71] or akin to the properties of the so-called chaotic breathers [72,73].

IV. RESULTS II: SIEVING THROUGH THE POPULATION OF BURSTS FOR ILMs

The wavelet-based procedure described in this work allows one to build and characterize ensembles of nonlinear excitations that increasingly populate the gap as the temperature is raised. Even though these soft excitations display distinct ILM-like features, such as the apparent ability to gather some energy from the background and self-stabilize during their lifetime beyond the equipartition law, it is hard to state whether such bursts are indeed instances of ILM excitation. In fact, according to the general arguments developed by Sievers
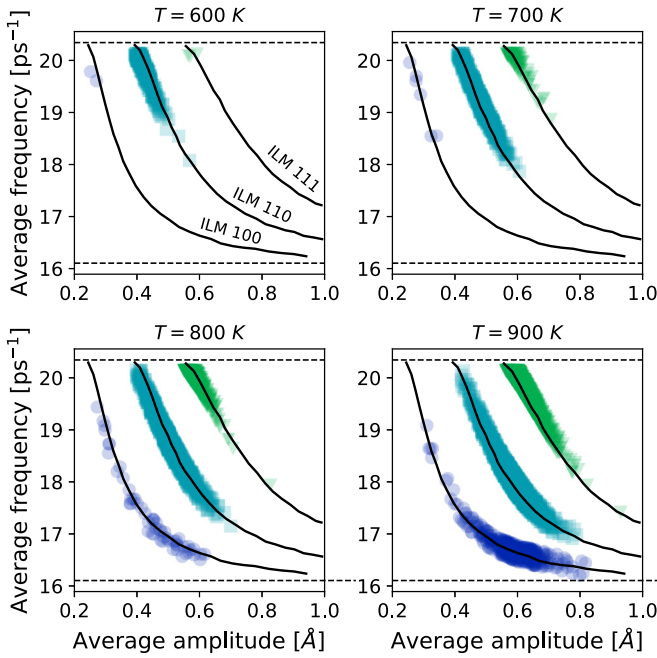
FIG. 6. Illustration of the procedure employed for sifting possible ILM-like excitations through the whole ensembles of bursts in the gap. At each temperature, [100], [110], and [111] subensembles are created (transparent circles) by keeping only the bursts closer than 1% to the corresponding theoretical ILMs [43] (solid lines) in the frequency-amplitude plane.

and co-workers in Ref. [41], the site-occupancy probability of a *thermal* ILM is expected to be very low—about 0.02 for a [111] excitation in 3D NaI at $T = 900$ K. While numerical analogues of exquisitely nonlinear experimental techniques such as discussed in Ref. [74] would be powerful tools to address this question, it also makes sense to turn to theoretical predictions for $T = 0$ excitations as possible *templates*, against which the raw ensembles of gap bursts can be *sifted*.

The theoretical ILM frequency-amplitude relations reported in Ref. [43] are shown as solid lines in Fig. 6 for the three ILM polarizations, [100], [110], and [111]. At each temperature, we sifted through the whole collection of bursts and assembled three subpopulations by keeping only those excitations whose distance from the theoretical curves was less than 1%. Practically, for each burst, we recovered the three theoretical frequencies corresponding to its measured average amplitude. The burst was then kept under the appropriate polarization label if the relative difference between its average frequency and the theoretical frequency was less than 1%. We observe that this is a rather crude scheme, as each burst is associated with a single Cartesian direction. Therefore, while this procedure makes perfect sense for the [100] polarization, it might be objected that by doing this we are not enforcing the additional correlations among different Cartesian directions required by the assumed polarizations. Of course, a burst found along x that would correspond to a genuine ILM polarized along the [110] direction would most likely match *to some extent* a burst on the same ion along the y direction. However, this is a tricky matter, as the phase relation between the two directions might be such that the two bursts would not necessarily appear correlated, depending on

TABLE II. Best-fit values of the energy and entropy differences describing the equilibrium between energy fluctuations and stabilized bursts according to the law (9), with $\Delta f = \Delta \epsilon - T \Delta s$. The excitations labeled according to different polarizations correspond to the subpopulations sieved out at each temperature from the whole ensemble of bursts by keeping only the excitations that match the corresponding theoretical frequency-amplitude relations taken from Ref. [43] (see again Fig. 6).

Excitation kind	$\Delta\epsilon$ (eV)	Δs (k_B)
All	0.54 ± 0.01	9 ± 0.2
[100]	1.16 ± 0.06	11.4 ± 0.8
[110]	0.32 ± 0.01	2.5 ± 0.2
[111]	1.06 ± 0.04	11.9 ± 0.5

the spectral resolution and on the burst lifetime itself. While conceiving the appropriate tool to enforce such constraints as rigorously as possible, we are nonetheless reporting here some interesting results obtained with the simplest sieving procedure outlined above.

Direct inspection of Fig. 6 shows that the number of putative ILM excitations increases with temperature. Moreover, it seems that the excitations that fall on the [110] theoretical curves are much more abundant than the [100] and [111] excitations, despite that the theory developed in Ref. [43] predicted the [111] modes to be the most stable ones. However, it should be remarked that the lifetime $\approx 3 \times 10^{-9}$ s, predicted in Ref. [43] for the [111] modes based on the interaction with a (Bose-Einstein) thermal distribution of phonons, exceeds by two orders of magnitude the longest lifetimes assigned to a burst in the gap in this study (about 30 ps).

The top left panel in Fig. 7 compares the site-occupancy probabilities relative to the ILM subpopulations to the global site-occupancy probability of the whole burst database. The data are well fitted by general chemical equilibria between two free-energy minima (possibly separated by a number of intermediates), embodied by expression (9). The corresponding free-energy differences are reported in Table II. It can be appreciated that putative ILM excitations along [100] and [111] appear to be rather in the minority with respect to *generic* burst excitations. Putative [110] modes seem to be more numerous at low and intermediate temperature. Nonetheless, the population of these kind of excitations seem to increase with temperature as that of the generic bursts, while [100] and [111] modes appear to be about three orders of magnitude less than generic bursts at intermediate temperatures, while surging in number with temperature much more rapidly than [110] modes. This is reflected by the best-fit value of the enthalpy and entropy differences (see Table II). Putative [100] and [111] ILM-like bursts seem far easier to excite from the point of view of entropy than [110] excitations, explaining the marked temperature dependence of their SOP. It is interesting to observe that the predictions made in Ref. [41] for [111] modes seem to underestimate the excitation entropy difference (4 k_B versus 12 k_B), which results in a reduced temperature dependence of their excitation equilibrium (dashed line in the top left panel of Fig. 7). This might indicate that in general at thermal equilibrium there might be more excitation channels than merely specified by the symmetry-equivalent
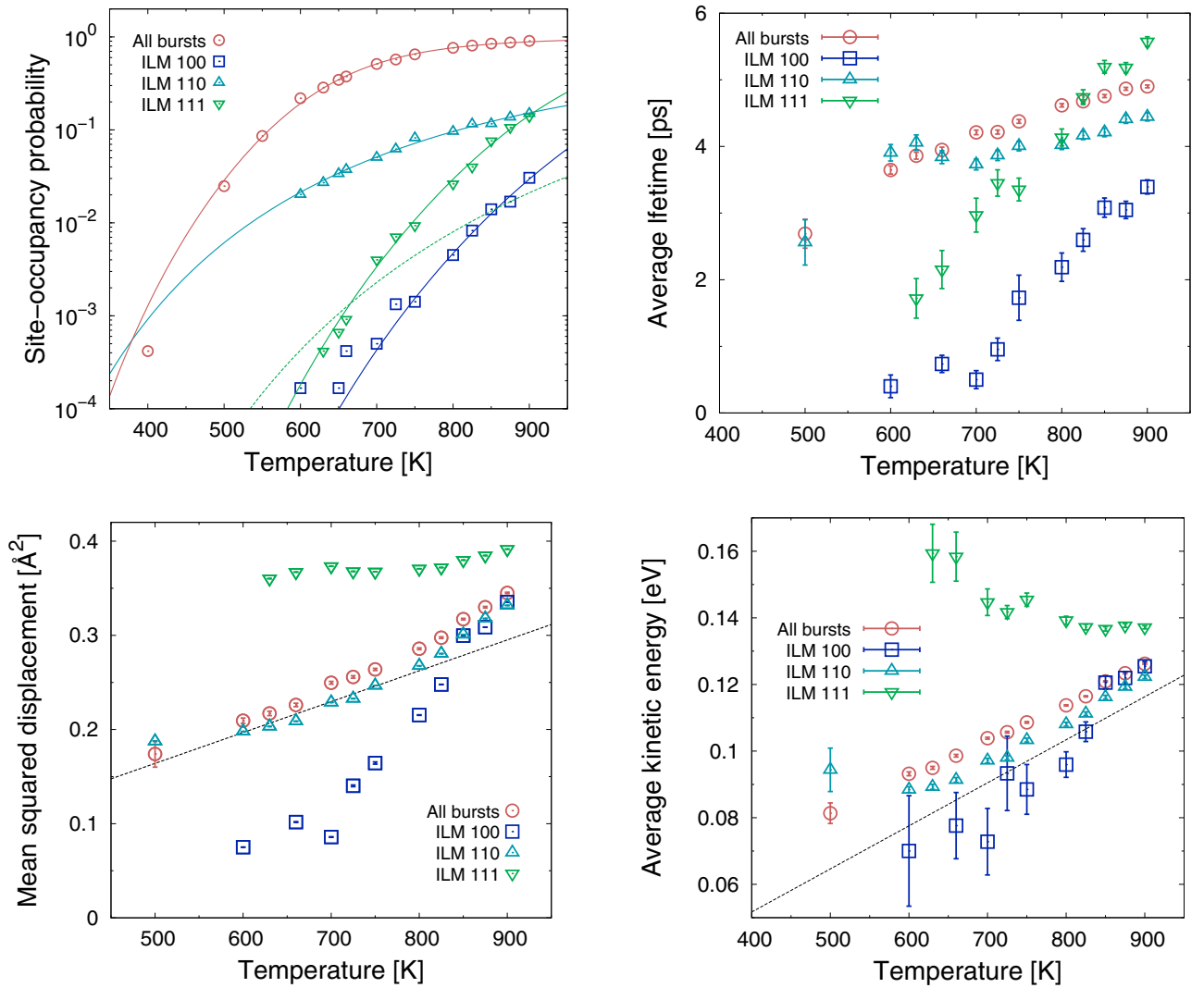
FIG. 7. Burst analysis for the putative ILM subpopulations compared to the data for the whole burst ensemble. (Top left) Site-occupancy probabilities and fits with the expression (9). The corresponding best-fit parameters are reported in Table II. The green dashed line is the SOP computed in Ref. [41] for [111] ILM excitations. (Top right) Average lifetime. (Bottom left) Mean-square displacement. The dashed line represents the average computed over the whole set of Na ions in the crystal. (Bottom right) Average kinetic energy. The dashed line marks the equipartition result. As expected, this describes the average kinetic energy of Na ions when computed over the whole set of Na ions in the crystal.

points at the boundary of the Brillouin zone (L points in the case of [111] modes). These might reflect interconversion events or mixed-character modes, as already suggested in Ref. [44].

An analysis of the lifetimes measured for putative ILM-like excitations also confirms some of the predictions made in Ref. [43] (top right panel in Fig. 7). Excitations along [100] and [110] display lower-than-average lifetimes, while the lifetimes of [111] excitations increase rapidly with temperature, to last beyond average bursts at high temperatures. Interestingly, the lifetimes of [100] and [111] bursts seem to display a marked dependence on temperature, matched by their rapidly increasing SOP, while [110] excitations show nearly temperature-independent lifetimes, rhyming with a much more slowly increasing SOP (top left panel). This seems to point to a less marked nonlinear character for bursts sieved out along [110].

Amplitudes and energies of bursts seem to trace a consistent picture (bottom panels in Fig. 7). While along [110], and to a lesser extent along [100], the data relative to the putative theoretical subpopulations display trends that are consistent with the average behavior of the whole burst database, the [111] subensemble demonstrates a substantially contrasting trend. More specifically, excitations selected to lie along the theoretical [111] dispersion law display systematically higher-than-average energies and larger-than-average amplitudes. This is consistent with a more marked nonlinear character of these excitations, which in turn upholds the predictions reported in Ref. [43] concerning the markedly higher lifetime of [111] ILMs.

V. CONCLUSIONS AND DISCUSSION

In this paper, we have introduced a method to resolve transient localization of energy in time-frequency space. Our

technique is based on continuous wavelet transform of velocity time series coupled to a threshold-dependent filtering procedure to isolate excitation events from background noise in a specific spectral region. A frequency integration in the reference spectral region allows us to track the time evolution of the center-of-mass frequency of that region. These reduced data, in turn, can be easily exploited to investigate the statistics of the burst excitation dynamics. For example, this procedure can be employed to characterize the distribution of the burst lifetimes and investigate the roots of the excitation process by looking at the distribution of excitation times (time intervals separating consecutive excitation events).

As an illustration of our method, we have employed the wavelet-based energy burst imaging technique to investigate spontaneous localization of nonlinear modes in the gap of NaI crystals at high temperature. Our method allows one to build a database of excitation events, and to measure their site-occupancy probability, average lifetime, energy, frequency, amplitude, and excitation times. It is highly likely that such database contains subpopulations corresponding to spontaneous excitation of ILMs, provided a sufficient number of events is recorded, i.e., provided large enough systems are considered and long-enough trajectories are simulated. Overall, the burst database shows rather clearly that the events recorded are thermally excited. One way to rationalize the overall excitation equilibrium and kinetics is in terms of a reaction kinetic scheme involving chemical species equivalents, representing *fluctuations* (F), *bursts* (B) along with a variable number of intermediates. The numerically measured lifetimes and excitation times suggest that such kind of reaction scheme is associated with an energy landscape with as many minima as different virtual species. It is possible that this analogy could be pushed even farther than this, through the identification of the appropriate collective coordinates (the support of the energy landscape), which could allow one to reconstruct the landscape from the simulations through standard free-energy calculation algorithms.

The problem than one faces in the second logical stage of our method is how to single out events corresponding to *genuine* ILM excitation, as opposed to generic soft nonlinear phonon excitations. We observe that this is a rather formidable task, as the fraction of such events is expected to be low, while their polarization and localization length can only be guessed from zero-temperature calculations. In this paper, we have followed a very simple and minimalistic strategy, based explicitly on the zero-temperature predictions, to sift through the whole burst database at each temperature in the quest for ILM events. This procedure seems to succeed, at least partially, in the task of isolating events that display a marked nonlinear character. In particular, events selected from the burst database by matching the theoretical $T = 0$ frequency-amplitude relation for the [111] polarization seem to detach the most from the average behavior of the entire databases, suggesting that at least some of these events might be genuine ILMs along [111]. The corresponding site-occupancy probability for these events is described by the same theoretical expression as suggested in Ref. [41], although we find that there might be more excitation pathways for these modes than merely specified by the symmetry-equivalent points at the

boundary of the Brillouin zone (L points). This might reflect interconversion events or mixed-character modes, as hinted at in Ref. [44].

From a general point of view, it is hard to state whether thermal populations of ILMs in crystals allow them to be detected and characterized directly from equilibrium MD simulations. It is possible that this would require, in general, some sort of an intrinsically nonlinear pump-probe technique to enhance selectively thermal populations of nonlinear excitations. A clever example of amplification and counting of ILM excitations is reported in Ref. [75] for quasi-one-dimensional antiferromagnetic lattices, where an original pump-probe technique based on a four-wave mixing amplification of the weak signal from the few large-amplitude ILMs is used to count ILM emission events. In principle, an ILM generation and steady-state locking techniques such as further discussed in Ref. [74] could be implemented numerically to produce energy localization in a controlled fashion in atomic lattices at high temperature.

In general, ILM localization is expected to be accompanied by a strain field (sometimes referred to as the dc component) as a result of odd-order anharmonic terms. Moreover, as suggested in Ref. [46], the strain field associated with thermal excitation of ILMs is expected to take the form of planar faultlike structures with an occurrence frequency f of approximately one in every ten cells ($f = 1/10$). However, our method is based on the analysis of velocity time series. Therefore it is insensitive in principle to static distortions associated with the ILM displacement fields. Nonetheless, we observe that a *spatial* version of our method could be designed in principle to detect the features of the strain fields associated with ILMs, by Gabor transforming spatial-Fourier transformed time series corresponding to specific wave vectors. To make contact with the results reported in Ref. [46], one should also consider larger systems including at least twice as many cells in each directions than the present study.

Although we demonstrated here the power of wavelet-based imaging to investigate the dynamics of nonlinear excitations in the gap of NaI crystals, methods of the like can be useful in many contexts where one wishes to characterize transient energy excitation or energy transfer processes. The latter kind of phenomena, which is not investigated here, appears to be a promising domain of application of our method, both at the classical and quantum level. For example, it would be interesting to adopt a tool inspired to our method to characterize the dynamics of energy transfer and exciton-phonon interactions in light-harvesting complexes [76–78]. Wavelet-based methods could be used to characterize the dynamics of vibrational energy transfer [79,80] in many complex system, including biomolecules. For example, coupled to pump-probe molecular dynamics approaches [81] to investigate in a time-resolved manner long-range coupling [82] in frequency space. These analysis could provide important information as to the structural and dynamical determinants of allosteric communication in proteins [83]. More generally, our method could make it possible to reconstruct the topology of the network of nonlinear interactions in a normal-mode space that is dual to the geography of energy redistribution in 3D space in many-body systems [84].

[1] J. L. Marín, S. Aubry, and L. M. Floría, Physica D **113**, 283 (1998).

[2] S. Flach and A. V. Gorbach, Phys. Rep. **467**, 1 (2008).

[3] R. S. MacKay and S. Aubry, Nonlinearity **7**, 1623 (1994).

[4] A. J. Sievers and S. Takeno, Phys. Rev. Lett. **61**, 970 (1988).

[5] J. Ford, Phys. Rep. **213**, 271 (1992).

[6] S. V. Dmitriev, A. P. Chetverikov, and M. G. Velarde, Phys. Status Solidi B **252**, 1682 (2015).

[7] S. A. Kiselev and A. J. Sievers, Phys. Rev. B **55**, 5755 (1997).

[8] V. Hizhnyakov, M. Haas, M. Klopov, and A. Shelkan, Lett. Mater. **6**, 61 (2016).

[9] J. L. Marin, F. M. Russell, and J. C. Eilbeck, Phys. Lett. A **281**, 21 (2001).

[10] E. Barani, E. A. Korznikova, A. P. Chetverikov, K. Zhou, and S. V. Dmitriev, Phys. Lett. A **381**, 3553 (2017).

[11] I. Evazzade, M. R. Roknabadi, M. Behdani, F. Moosavi, D. Xiong, K. Zhou, and S. V. Dmitriev, Eur. Phys. J. B **91**, 163 (2018).

[12] A. Fraile, E. N. Koukaras, K. Papagelis, N. Lazarides, and G. P. Tsironis, Chaos Solitons Fractals **87**, 262 (2016).

[13] V. Hizhnyakov, M. Klopov, and A. Shelkan, Phys. Lett. A **380**, 1075 (2016).

[14] R. T. Murzaev, D. V. Bachurin, E. A. Korznikova, and S. V. Dmitriev, Phys. Lett. A **381**, 1003 (2017).

[15] J. A. Sepulchre and R. S. MacKay, Physica D **113**, 342 (1998).

[16] G. Kopidakis and S. Aubry, Physica D **130**, 155 (1999).

[17] G. Kopidakis and S. Aubry, Physica D **139**, 247 (2000).

[18] *Nonlinear Excitations in Biomolecules*, edited by M. Peyrard (Springer-Verlag, Berlin, Heidelberg, 1995).

[19] B. Juanico, Y. H. Sanejouand, F. Piazza, and P. De Los Rios, Phys. Rev. Lett. **99**, 238104 (2007).

[20] F. Piazza and Y.-H. Sanejouand, Phys. Biol. **5**, 026001 (2008).

[21] S. Iubini, R. Franzosi, R. Livi, G.-L. Oppo, and A. Politi, New J. Phys. **15**, 023032 (2013).

[22] V. I. Dubinko, J. F. R. Archilla, S. V. Dmitriev, and V. Hizhnyakov, in *Quodons in Mica: Nonlinear Localized Traveling Excitations in Crystals*, edited by J. Archilla, N. Jimenez, V. Sanchez Morcillo, and L. Garcia Raff, Springer Series in Materials Science Vol. 221 (Springer International Publishing, Switzerland, 2015), pp. 381–398.

[23] V. I. Dubinko and D. V. Laptev, Lett. Mater. **6**, 16 (2016).

[24] V. I. Dubinko and F. Piazza, Lett. Mater. **4**, 273 (2014).

[25] M. V. Ivanchenko, O. I. Kanakov, V. D. Shalfeev, and S. Flach, Physica D **198**, 120 (2004).

[26] M. Eleftheriou and S. Flach, Physica D **202**, 142 (2005).

[27] Y. Ming, D. B. Ling, H. M. Li, and Z. J. Ding, Chaos **27**, 063106 (2017).

[28] J. A. Baimova, R. T. Murzaev, and A. I. Rudskoy, Phys. Lett. A **381**, 3049 (2017).

[29] J. A. Baimova, R. T. Murzaev, I. P. Lobzenko, S. V. Dmitriev, and K. Zhou, J. Exp. Theor. Phys. **122**, 869 (2016).

[30] A. A. Kistanov and S. V. Dmitriev, Phys. Solid State **54**, 1648 (2012).

[31] P. Binder, D. Abraimov, A. V. Ustinov, S. Flach, and Y. Zolotaryuk, Phys. Rev. Lett. **84**, 745 (2000).

[32] E. Trias, J. J. Mazo, and T. P. Orlando, Phys. Rev. Lett. **84**, 741 (2000).

[33] J. W. Steeds, F. M. Russell, and W. J. Vine, Optik **92**, 149 (1993).

[34] F. M. Russell, in *Quodons in Mica: Nonlinear Localized Traveling Excitations in Crystals*, edited by J. Archilla, N. Jimenez, V. Sanchez Morcillo, and L. Garcia Raff, Springer Series in Materials Science Vol. 221 (Springer, Berlin, 2015), pp. 3–33.

[35] J. L. Marin, J. C. Eilbeck, and F. M. Russell, Phys. Lett. A **248**, 225 (1998).

[36] F. M. Russell, J. F. Archilla, F. Frutos, and S. Medina-Carrasco, Europhys. Lett. **120**, 46001 (2017).

[37] M. E. Manley, M. Yethiraj, H. Sinn, H. M. Volz, A. Alatas, J. C. Lashley, W. L. Hults, G. H. Lander, and J. L. Smith, Phys. Rev. Lett. **96**, 125501 (2006).

[38] M. E. Manley, A. Alatas, F. Trouw, B. M. Leu, J. W. Lynn, Y. Chen, and W. L. Hults, Phys. Rev. B **77**, 214305 (2008).

[39] R. T. Murzaev, R. I. Babicheva, K. Zhou, E. A. Korznikova, S. Y. Fomin, V. I. Dubinko, and S. V. Dmitriev, Eur. Phys. J. B **89**, 168 (2016).

[40] M. E. Manley, A. J. Sievers, J. W. Lynn, S. A. Kiselev, N. I. Agladze, Y. Chen, A. Llobet, and A. Alatas, Phys. Rev. B **79**, 134304 (2009).

[41] A. J. Sievers, M. Sato, J. B. Page, and T. Rössler, Phys. Rev. B **88**, 104305 (2013).

[42] L. Z. Khadeeva and S. V. Dmitriev, Phys. Rev. B **81**, 214306 (2010).

[43] D. Nevedrov, V. Hizhnyakov, and A. J. Sievers, Anharmonic gap modes in alkali halides, in *Vibronic Interactions: Jahn-Teller Effect in Crystals and Molecules*, edited by M. D. Kaplan and G. O. Zimmerman (Springer Netherlands, Dordrecht, 2001), pp. 343–347.

[44] M. E. Manley, D. L. Abernathy, N. I. Agladze, and A. J. Sievers, Sci. Rep. **1**, 4 (2011).

[45] M. Kempa, P. Ondrejkovic, P. Bourges, P. Marton, and J. Hlinka, Phys. Rev. B **89**, 054308 (2014).

[46] M. E. Manley, J. R. Jeffries, H. Lee, N. P. Butch, A. Zabalegui, and D. L. Abernathy, Phys. Rev. B **89**, 224106 (2014).

[47] S. Plimpton, J. Comput. Phys. **117**, 1 (1995).

[48] A. R. Ruffa, Phys. Rev. **130**, 1412 (1963).

[49] J. E. Rapp and H. D. Merchant, J. Appl. Phys. **44**, 3919 (1973).

[50] M. J. L. Sangster, Solid State Commun. **18**, 67 (1976).

[51] J. K. Jain, J. Shanker, and D. P. Khandelwal, Phys. Rev. B **13**, 2692 (1976).

[52] M. J. L. Sangster, R. M. Atwood, and U. Schröder, J. Phys. C: Solid State Phys. **11**, 1523 (1978).

[53] J. Shanker, J. Narain, and A. K. Rajauria, Phys. Status Solidi B **122**, 435 (1984).

[54] J. Shanker and G. G. Agrawal, Phys. Status Solidi B **123**, 11 (1984).

[55] M. Kumar, A. J. Kaur, and J. Shanker, J. Chem. Phys. **84**, 5735 (1986).

[56] A. M. Sherry and M. Kumar, J. Phys. Chem. Solids **52**, 1145 (1991).

[57] K. Sunil and B. S. Sharma, Indian J. Pure Appl. Phys. **50**, 387 (2012).

[58] P. P. Ewald, Ann. Phys. **369**, 253 (1921).

[59] A. Muller, Proc. R. Soc. London A **154**, 624 (1936).

[60] J. G. Kirkwood, Z. Phys. (Leipzig) **33**, 57 (1932).

[61] J. H. Harding, *Computer Simulation in Materials Science: Interatomic Potentials, Simulation Techniques, and Applications*, edited by M. Meyer and V. Pontikis (Kluwer, Dordrecht, 1991).

[62] S. Nosé, Mol. Phys. **52**, 255 (1984).

[63] W. G. Hoover, Phys. Rev. A **31**, 1695 (1985).

[64] J. D. Gale and A. L. Rohl, Mol. Simul. **29**, 291 (2003).

[65] K. Forinash and W. Lang, Physica D **123**, 437 (1998).

[66] D. Gabor, J. Inst. Elec. Eng. (London) **93 (III)**, 429 (1946).

[67] T. Cretegny, R. Livi, and M. Spicci, Physica D **119**, 88 (1998).

[68] L. Z. Khadeeva and S. V. Dmitriev, Phys. Rev. B **84**, 144304 (2011).

[69] S. Flach, K. Kladko, and R. S. MacKay, Phys. Rev. Lett. **78**, 1207 (1997).

[70] M. Kastner, Nonlinearity **17**, 1923 (2004).

[71] F. Piazza, S. Lepri, and R. Livi, Chaos **13**, 637 (2003).

[72] T. Cretegny, T. Dauxois, S. Ruffo, and A. Torcini, Physica D **121**, 109 (1998).

[73] Y. A. Kosevich and S. Lepri, Phys. Rev. B **61**, 299 (2000).

[74] J. P. Wrubel, M. Sato, and A. J. Sievers, Phys. Rev. Lett. **95**, 264101 (2005).

[75] M. Sato and A. J. Sievers, Phys. Rev. B **71**, 214306 (2005).

[76] S. Pouyandeh, S. Iubini, S. Jurinovich, Y. Omar, B. Mennucci, and F. Piazza, Phys. Biol. **14**, 066001 (2017).

[77] L. Viani, M. Corbella, C. Curutchet, E. J. O'Reilly, A. Olaya-Castro, and B. Mennucci, Phys. Chem. Chem. Phys. **16**, 16302 (2014).

[78] J. Wu, F. Liu, Y. Shen, J. Cao, and R. J. Silbey, New J. Phys. **12**, 105012 (2010).

[79] X. Yu and D. Leitner, J. Phys. Chem. B **107**, 1698 (2003).

[80] D. M. Leitner, Annu. Rev. Phys. Chem. **59**, 233 (2008).

[81] K. Sharp and J. J. Skinner, Proteins: Structure, Function, Bioinformatics **65**, 347 (2006).

[82] F. Piazza and Y.-H. Sanejouand, Europhys. Lett. **88**, 68001 (2009).

[83] C.-J. Tsai and R. Nussinov, PLoS Comput. Biol. **10**, e1003394 (2014).

[84] A. Allain, I. Chauvot de Beauchene, F. Langenfeld, Y. Guarracino, E. Laine, and L. Tchertanov, Faraday Discuss. **169**, 303 (2014).